Chemical Science

ROYAL SOCIETY OF CHEMISTRY

EDGE ARTICLE

View Article Online
View Journal | View Issue

Cite this: *Chem. Sci.*, 2021, **12**, 3944

All publication charges for this article have been paid for by the Royal Society of Chemistry

Received 14th December 2020
Accepted 21st January 2021

DOI: 10.1039/d0sc06837c

rsc.li/chemical-science

Translational dynamics of a non-degenerate molecular shuttle imbedded in a zirconium metal–organic framework†

Benjamin H. Wilson,[a] Louae M. Abdulla,[a] Robert W. Schurko *[bc] and Stephen J. Loeb *[a]

A new [2]rotaxane molecular shuttle linker based on the binding of a 24-crown-8 ether macrocycle at a benzimidazole recognition site was synthesised. The shuttling dynamics of the linker were studied in solution and the structure confirmed by X-ray crystallography. A multivariate Zr(IV) MOF, **UWDM-11**, containing the new MIM linker and primary linker tetramethylterphenyldicarboxylate was synthesised and the translational motion of the molecular shuttle studied in the solid state. The use of a ^{13}C enriched MIM linker allowed the dynamics of both activated and mesitylene-solvated **UWDM-11** to be elucidated by VT ^{13}C CPMAS SSNMR. The incorporation of mesitylene into the pores of **UWDM-11** resulted in a significant increase in the barrier for thermally driven translation of the macrocycle.

Introduction

Mechanically interlocked molecules (MIMs) are assemblies composed of two or more molecular components linked by a mechanical bond.[1] The translation or rotation of the individual components relative to one another provides MIMs with a high degree of conformational freedom and makes them ideal for inclusion in artificial molecular machines.[2–5]

Rotaxanes are a class of MIM comprised of a macrocyclic wheel and an axle with bulky stoppers to give a dumbbell.[2] If there are multiple recognition sites along the axle which are accessible to the wheel, back and forth translational motion of the macrocycle between the sites can occur – this type of MIM is referred to as a molecular shuttle.[3] When both recognition sites for the wheel are identical, the energy barriers for moving back and forth from one site to the other are equivalent, in which case, the system is said to be a degenerate molecule shuttle.[4] However, when the recognition sites are different, the system is referred to as a non-degenerate molecular shuttle, as the energy barriers for moving back and forth from one site to the other are now inequivalent and the translational dynamics more complex.[5]

The dynamics of MIMs such as molecular shuttles are most often studied in solution.[5d,6] However, if functional materials containing MIMs are to be realised,[7] the factors affecting their rotational and translational motion in the solid state must be thoroughly understood. Metal–organic frameworks (MOFs) are an ideal candidate for the synthesis of solid-state materials containing MIMs due to the periodic arrangement of the organic linkers and their inherent porosity which provides the free volume necessary for observation of MIM dynamics.[8] It has also been demonstrated that the inclusion of guest molecules can influence the dynamic behaviour of the linkers.[9] Ligands containing [2]rotaxanes can be designed in a variety of ways with examples known that show both rotation and translation of the macrocycle.[8d,10] We have previously reported MOFs, **UWDM-4**,[10h] **UWDM-8**,[11] and **UWDM-9**[11] which contain degenerate molecular shuttles and studied their dynamics in the solid state (*e.g.*, Fig. 1a). In particular, the Zn(II) based MOF, **UWDM-4**, required solvent molecules (xylenes) in the pores to retain the material's crystallinity. It was observed that the barrier to translational (14.1 kcal mol^{-1}) in the solvated MOF was considerably higher than that found for the free MIM in solution (7.7 kcal mol^{-1}). This difference was likely due to the increased effective viscosity of solvent molecules confined in the framework.[10h] Recently, we have focused on more robust Zr(IV) based MOFs because of their excellent chemical and thermal stabilities.[12] This should facilitate the study of both the activated and solvated forms of the MOFs and allow us to gain a better understanding of the role of guest molecules in the translational dynamics of the macrocycle (*vide infra*). Furthermore, the enhanced chemical stability of Zr(IV) MOFs introduces the possibility of controlling the dynamics *via* external chemical stimuli;[13] for instance, the benzimidazole core of the molecular

[a]*Department of Chemistry and Biochemistry, University of Windsor, Windsor, Ontario, N9B 3P4, Canada. E-mail: loeb@uwindsor.ca*

[b]*Department of Chemistry and Biochemistry, Florida State University, Tallahassee, FL, 32306, USA*

[c]*National High Magnetic Field Laboratory, Tallahassee, FL 32310, USA*

† Electronic supplementary information (ESI) available: Synthesis and characterization of all new precursors and molecular shuttles; MOF synthesis; solution and solid-state NMR experiments; X-ray diffraction experiments. CCDC 2049899–2049901. For ESI and crystallographic data in CIF or other electronic format see DOI: 10.1039/d0sc06837c

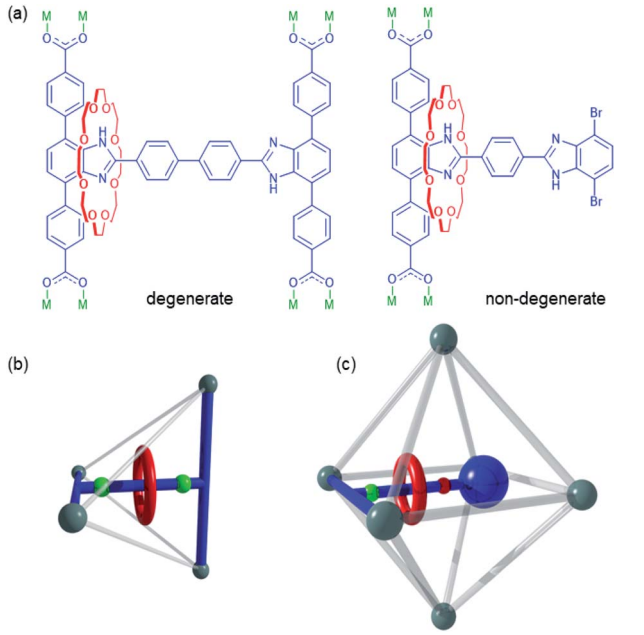

Fig. 1 (a) The degenerate molecular shuttle (left) previously incorporated into the Zr(IV) MOF **UWDM-8** and the non-degenerate molecular shuttle (right) incorporated into **UWDM-11**; this work. (b) A schematic representation of the tetrahedral cavity of **UWDM-8** crosslinked with a degenerate molecular shuttle. (c) The octahedral cavity of **UWDM-11** featuring a non-degenerate molecular shuttle appended to one of the linkers.

shuttle featured in this work is particularly sensitive to changes in pH.[14]

Previously reported Zr(IV) MOFs **UWDM-8** and **UWDM-9**[11] contain an H-shaped tetracarboxylate [2]rotaxane ligand that crosslinks the tetrahedral cavity of **fcu** MOFs of the **UiO-68** family (Fig. 1b).[15] Despite trials with a variety of primary linkers (*i.e.*, derivatives of terphenyldicarboxylic acid), the tetrahedral cavity was found to be too sterically encumbered for simple translation of the molecular shuttle to occur.[11] Although the octahedral cavity of an **fcu** MOF is far less sterically restricted, making it a significantly better candidate for the imbedding of a molecular shuttle, the separation of parallel linkers forming the edges of the octahedral cavities is such that there is not a simple symmetrical H-shaped linker capable of spanning the cavity. An alternative approach would be to design a linker that simply protrudes into the cavity rather than spanning it completely. Ideally, this linker would be too large to fit into the tetrahedral cavity of the MOF but small enough to fit into the larger octahedral cavity (Fig. 1c).

Herein, we present the design and synthesis of an H-shaped dicarboxylate linker containing a non-degenerate molecular shuttle and its incorporation into the octahedral cavities of a Zr(IV) MOF with an **fcu** net. This non-degenerate molecular shuttle introduces a greater degree of complexity to the translational motion of the macrocycle, as the two chemically distinct recognition sites have different affinities for the macrocycle. Variable-temperature (VT) ^{1}H–^{13}C cross-polarization magic-angle spinning (CP/MAS) solid-state NMR (SSNMR) was used to study the translational motion of the macrocycle in the octahedral cavity for both the activated and solvated forms of this new MOF, **UWDM-11**.

Results and discussion

Synthesis and characterisation of H-shaped molecular shuttle

The MIM linker was synthesised as the diester, **2**, from the protonated T-shaped axle, [**H1**][BF_4], by first forming the pseudorotaxane [**H1**⊂**24C8**][BF_4]; Scheme 1. Capping to make the [2]rotaxane was achieved by adding a dibromo-benzimidazole stopper under mild conditions using $ZrCl_4$ as a Lewis acid catalyst; full synthetic procedures are detailed in the ESI.† The neutral [2]rotaxane **2** was isolated by the addition of excess triethylamine. Complete assignment of the ^{1}H NMR spectrum was aided by COSY and ROESY NMR techniques (Fig. S2–S4†). Compound **2*** was synthesised using the same protocol but with a ^{13}C enriched site at the 2-position of the benzimidazole to aid the characterisation of the shuttling behaviour in the MOF using VT ^{1}H–^{13}C CP/MAS SSNMR. The dicarboxylic acid linkers H_2**3** and H_2**3*** were prepared *via* ester hydrolysis under basic conditions.

For **2**, through-space correlations between the protons on the central phenyl ring of the axle and those on the macrocycle were detected by ROESY experiments however, no correlations between the **24C8** ring and phenyl protons of the terphenyl stopper were detected due to the rapid dynamic behaviour of the macrocycle (Fig. S3†). In the case of **2***, only a single peak was observed in the room temperature ^{13}C NMR spectrum of the ^{13}C enriched site of the labelled benzimidazole group, since the

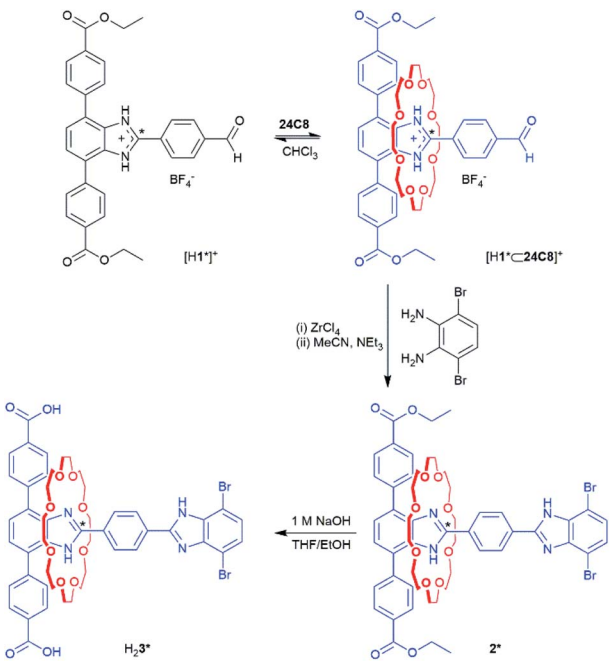

Scheme 1 The reactions utilised to synthesise the non-degenerate MIM linker H_2**3** and its ^{13}C enriched analog. Note, unlike previously reported symmetrical H-shaped linkers, only the terphenyl benzimidazole site is ^{13}C enriched (marked *).

shuttling motion is fast compared to the NMR timescale. Cooling **2*** to 210 K resulted in only a slight broadening and downfield shift of the peak (Fig. S8†). Based on previous observations of related H-shaped rotaxanes, the terphenyl-stoppered benzimidazole recognition site should be more energetically favourable due to the formation of extra C–H···O interactions between the aromatic hydrogen atoms of the terphenyl rings and the oxygen atoms of the crown ether macrocycle.[16] However, due to the rapid shuttling rates of **2** and **2*** in solution, the relative energetic stabilities of sites **a** (terphenyl stopper) and **b** (dibromo stopper) could not be elucidated.

The shuttling behaviour of the crown ether in these types of systems is particularly sensitive to pH. As **2** and **2*** are unsymmetrical, one benzimidazole site will have a higher preference for protonation and therefore binding of the crown ether. Addition of one equivalent of $HBF_4 \cdot Et_2O$ to **2** or **2*** results in mono-protonation of the benzimidazole at the terphenyl end of the molecule to give [**H2**][BF_4] and [**H2***][BF_4] respectively. Complete assignment of the ^{1}H NMR spectra for [**H2**]$^+$ was aided by COSY and ROESY NMR techniques (Fig. S5–S7†). The chemical shift for the ^{13}C enriched site of the benzimidazolium group in [**H2***]$^+$ is shifted downfield as expected (Fig. S10†) and through-space correlations between the protons on the phenyl rings of the stopper and the **24C8** macrocycle are now observed (Fig. S7†). Mono-protonation to give [**H2**]$^+$ and [**H2***]$^+$ results in recognition site **a** becoming significantly more energetically favourable than **b**, due to addition of a second hydrogen bond donor and a positive charge. Hence, the energy barrier for translational motion is too great for shuttling to occur at room temperature.

It is noted that accompanying the changes in the NMR spectra upon protonation is a qualitative change in the fluorescence of the MIM linker (Fig. S1†). The propensity of these types of molecules toward mono-protonation due to stabilizing hydrogen bonding from the crown ether often complicates experiments and the different fluorescent profiles of **2** and [**H2**]$^+$ are useful indicators of the protonation state.

Single crystals of neutral [2]rotaxane **2**·CH_3OH suitable for single-crystal X-ray diffraction (SC-XRD) were formed by slow evaporation of a CH_2Cl_2/CH_3OH solution (Fig. 2a, Table S1 and Fig. S11†). The macrocycle is bound to the less favourable dibromo site **b** by way of a single hydrogen bond between the N–H of the benzimidazole and an oxygen atom of the crown ether (Table S2†). In related degenerate molecular shuttles, hydrogen bonds between the phenyl ring protons of the terphenyl stoppered end stabilise the binding of the crown ether about the benzimidazole recognition site.[6a] It was therefore expected that the crown ether in **2** would be bound at recognition site **a**. The binding at site **b** is most likely a consequence of crystal packing as the benzimidazole of the terphenyl stoppered site participates in π-stacking interactions with benzimidazole moieties of neighbouring molecules, hindering the binding of the macrocycle at site **a** (Fig. S12 and S13†). The methanol molecule behaves as both a hydrogen bond acceptor for the N–H of the terphenyl benzimidazole moiety and a hydrogen bond donor for one of the oxygen atoms of the crown ether.

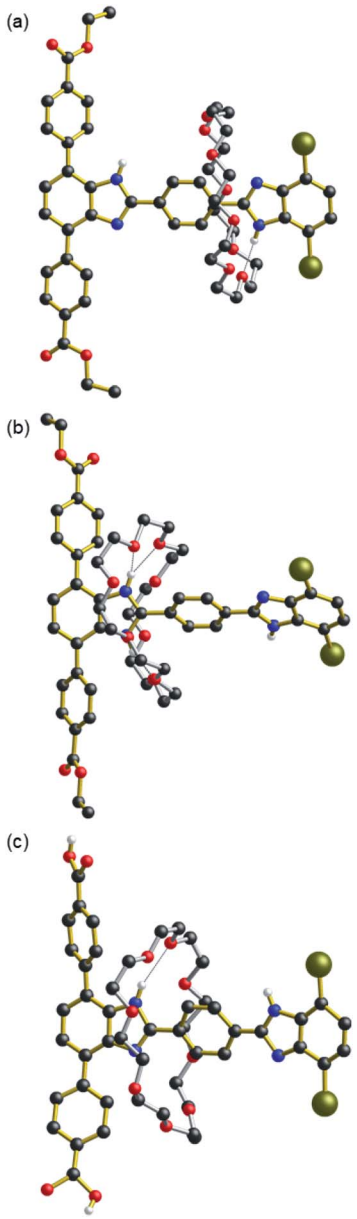

Fig. 2 Ball-and-stick representations of the single-crystal X-ray structures of (a) neutral [2]rotaxane diester **2**, (b) protonated [2]rotaxane diester [**H2**⊂**24C8**][BF_4] and (c) neutral [2]rotaxane diacid **3**. Colour key: green = bromine, red = oxygen, blue = nitrogen, black = carbon, white = hydrogen. BF_4 anions, solvent molecules and H-atoms not involved in primary H-bonds are omitted for clarity.

Single crystals of the protonated [2]rotaxane [**H2**][BF_4]·0.5(CH_3CN)·0.5(Et_2O) suitable for SC-XRD were formed by vapor diffusion of diethyl ether into an acetonitrile solution (Fig. 2b, S14 and Table S1†). Both of the mono-protonated rotaxanes in the unit cell feature the crown ether macrocycle binding at site **a**, indicating that it is this site which is protonated to become the benzimidazolium in agreement with the solution spectroscopic data. The binding of the macrocycle at this recognition site is stabilised by two sets of hydrogen bonding interactions occurring between the crown ether oxygen

atoms and the two N–H donors of the benzimidazolium group (Table S3†). Additional C–H···O interactions between the aromatic groups of the terphenyl stopper and the crown ether further stabilise this position. The salient difference between the two crystallographically unique rotaxanes is the nature of the interactions at the N–H group of the **b** recognition site; one is with a diethyl ether molecule while the other is with a tetrafluoroborate anion. Both of these entities behave as hydrogen bond acceptors to the benzimidazolium hydrogen bond donor (Fig. S14†).

Single crystals of the neutral [2]rotaxane diacid linker **3** were formed *via* slow evaporation of a DMF solution (Fig. 2c, S15 and Table S4†). Both molecules of **3** in the asymmetric unit feature the **24C8** macrocycle binding at the more favourable terphenyl recognition site **a**, in contrast to **2**, further highlighting the importance of packing interactions on the preference for **24C8** binding in the solid-state.

MOF synthesis and characterization

Dicarboxylate MIM ligands **3** and **3*** were designed such that the appended [2]rotaxane molecular shuttle would be directed into the octahedral cavity when the linker is incorporated into the parent MOF **PCN-57** (Fig. 3a). Our previous efforts to incorporate a molecular shuttle into **PCN-57** focused on using a tetracarboxylate MIM linker that cross-linked the tetrahedral cavity.[11] However, the dimensions of the octahedral cavity are such that a similar, symmetrical cross-linking ligand cannot be readily synthesised. We therefore, chose to utilise a dicarboxylate ligand with an appended rotaxane that is too large to fit into the tetrahedral cavity (based on modelling in Materials Studio[17] using the crystal structure of **PCN-57**[15b]) and should be oriented into the octahedral cavity (Fig. 3b).

The new multivariate MOF, **UWDM-11**, was synthesised under solvothermal conditions at 100 °C in DMF with a ratio of MIM linker H_2**3** to **TTDC** linker to $ZrCl_4$ of 1 : 4 : 6 with TFA as a modulator. This resulted in the formation of a white microcrystalline solid. Synthesis of MOFs under these conditions with this class of MIM linker inevitably produces a material which is in a mono-protonated state; *i.e.* [**UWDM-11**-H][TFA].[11] The as-synthesised MOF was thus soaked in an ethanol solution of proton sponge to ensure the rotaxane was fully converted to the neutral form. Solvent exchange with CH_2Cl_2 followed by heating at 120 °C under vacuum produced the neutral activated MOF, **UWDM-11**. TGA verified the lack of solvent molecules in the pores while the PXRD pattern matched that of the parent MOF, **PCN-57** (Fig. 3c and S19†). To confirm the presence of the MIM linker in the MOF, a sample was digested in $K_3PO_4/D_2O/d_6$-DMSO and the ratio of **3** to **TTDC** of 1 : 8 calculated from the solution ^{1}H NMR spectrum (Fig. S16†). This ratio indicates that, as intended, >95% of the octahedral cavities are occupied by an appended [2]rotaxane molecular shuttle. The thermal stability of the materials was confirmed by TGA (Fig. S17†) and VT-PXRD demonstrated that **UWDM-11** retained crystallinity up to 175 °C (Fig. S21†).

The rationale behind incorporating molecular shuttles into Zr-based MOFs is the high thermal and chemical stability of the material which allows for the pH sensitivity of the molecular shuttle to be exploited in the solid-state. A sample of **UWDM-11**

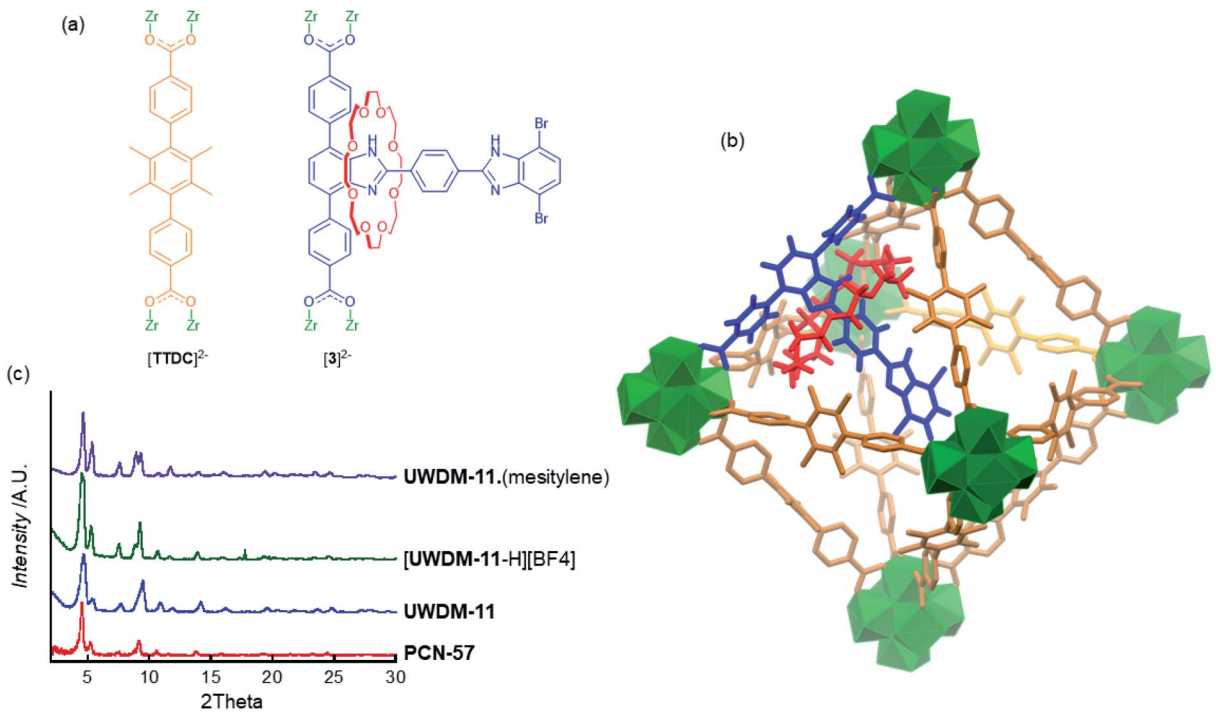

Fig. 3 (a) The two linkers used to construct the multivariate MOF **UWDM-11**; primary linker $[TTDC]^{2-}$ and [2]rotaxane $[3]^{2-}$. (b) A Molecular Studio (Forcite) geometry-optimised model of the octahedral cavity in **UWDM-11**; MIM axle = blue, **24C8** macrocycle = red, primary $[TTDC]^{2-}$ linkers = orange and $[Zr_6O_4(OH)_4]^{12+}$ nodes = green. (c) PXRD of **PCN-57** and various versions of **UWDM-11**.

was soaked in an ethanol solution of HBF_4 to give the mono-protonated framework, [**UWDM-11**-H][BF_4]. The integrity of the framework was confirmed *via* PXRD (Fig. 3c and S20†) as well as IR and a change in fluorescence (Fig. S18†).

It was postulated that the contents of the pores in **UWDM-11** would influence the dynamics of the molecular shuttle. Mesitylene was selected because of its high boiling point and low polarity. It was reasoned that this would limit competitive solvent interactions with the benzimidazole and crown ether and thus limit the solvent effects to an increase in the effective viscosity of the system.[9a] To this end, an activated (solvent free) sample of **UWDM-11** was loaded with mesitylene by soaking the material in mesitylene for 48 h to give **UWDM-11**·(mesitylene). PXRD showed retention of the framework integrity (Fig. 3c and S19†) while TGA provided insight into the amount of mesitylene absorbed (Fig. S19†). TGA of a sample of freshly filtered **UWDM-11**·(mesitylene) was performed while a second sample was left dry in a capped vial for 24 h and a second TGA measurement carried out. The as-synthesised sample showed mass loss of 50% between room temperature and 170 °C which constitutes the loss of 26 molecules of mesitylene from **UWDM-11**·(mesitylene). This can be attributed to a mix of surface adsorbed mesitylene and that from the pores of the MOF. The 24 h aged sample does not lose mass at room temperature but features a mass loss of 45% between 45 and 170 °C, which constitutes the loss of 21 molecules of mesitylene from inside the pores of **UWDM-11**·(mesitylene). This indicates that a significant number of molecules are retained in the framework when it is removed from the solvent.

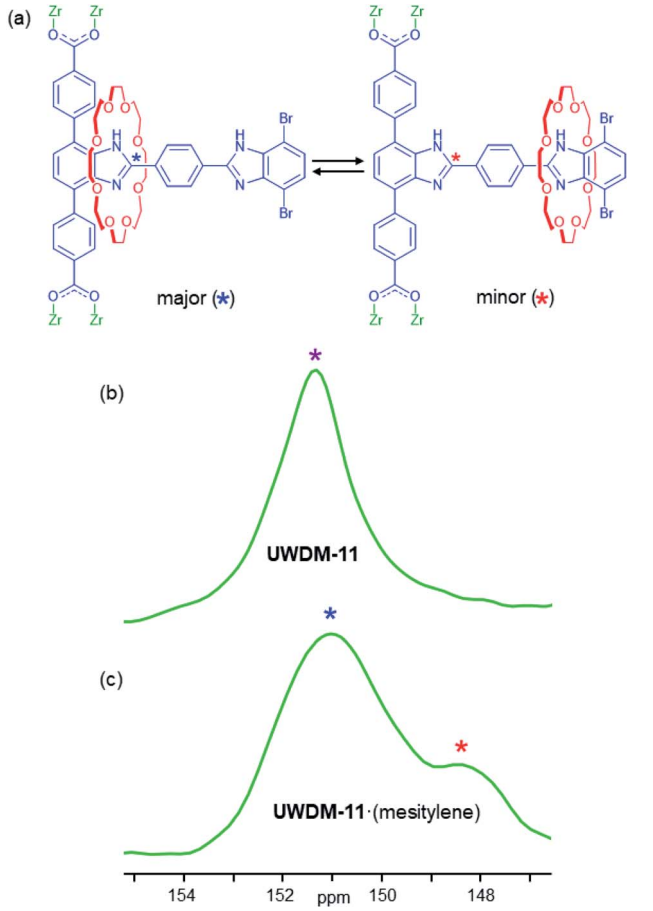

Fig. 4 (a) The two translational co-conformations possible for the non-degenerate, [2]rotaxane molecular shuttle **3** inside the pores of **UWDM-11**. The partial ^1H–^{13}C CP/MAS SSNMR spectra for (b) solvent-free **UWCM-11** (c) and **UWDM-11**·(mesitylene). Both spectra were recorded at 173 K and show the peak(s) corresponding to the ^{13}C enriched position (*) of the 4,7-diphenyl-benzimidazole moiety. For **UWDM-11**, only a single peak is observed for occupied and unoccupied sites corresponding to a weighted average chemical shift due to fast translation motion. For **UWDM-11**·(mesitylene), the shuttling motion is slowed, and two peaks are observed corresponding to the two possible co-conformations.

Solid-state NMR analysis

^1H–^{13}C CP-MAS ^{13}C SSNMR spectra of a solvent-free sample of **UWDM-11** were measured between 173 and 273 K. Each spectrum has a peak at 151.3 ppm corresponding to the ^{13}C-enriched site (marked with * in Fig. 4a) of the 4,7-phenyl substituted benzimidazole moiety (Fig. 4a and S22†). This single peak (Fig. 4b) corresponds to the weighted average chemical shift for the two possible co-conformations (*i.e.*, the crown ether is bound and unbound) and indicates that the ring is rapidly shuttling. As the shuttling of the crown ether macrocycle is faster than the NMR timescale, even at 173 K, an energy barrier for translation cannot be determined accurately. As the shuttling was shown to be fast in solution, it was expected that it would be at least as fast in the solid state for the activated MOF, as there are no solvent molecules present and there are no steric limitations imposed by the framework.

Previously, we have reported a higher energy barrier for shuttling in the solid state than in solution when the MOF contained guest molecules in the pores.[10h] Therefore, **UWDM-11**·(mesitylene) was also investigated to assess whether the presence of guest molecules could be used to slow the dynamics and allow characterisation of the shuttling rate in this material. The SSNMR spectra obtained at 173, 198 and 223 K show a broad peak at ~151 ppm with a shoulder at ~148 ppm (Fig. 4c, S23 and S25†). At 173 K, the intensity of the peak at 148 ppm is the highest; this intensity decreases with increasing temperature, and coalescence into a broad, lopsided peak is observed at 273 K. This peak shape remains relatively consistent until about 348 K where it becomes more symmetric and sharper, consistent with the rapid shuttling of the crown ether macrocycle occurring as the solvent molecules are lost at elevated temperature, as indicated by TGA (Fig. S19†).

This supports the idea that the inclusion of guest molecules in the pores of the MOF hinders the shuttling of the macrocycle compared to the fully activated MOF where the shuttling is at least as fast as in solution. This contrasts to recent studies by our group focusing on ring rotation as opposed to ring shuttling, which revealed ring rotation to be essentially independent of guest molecules.[10b] This is likely due to the difference in the types of motions. Rotation of a large macrocyclic ring can occur with very little displacement of solvent molecules, but the large amplitude translation of the ring from one site to another

requires a significant change in free volume around the two recognition sites which results in the displacement of guest molecules occupying those volumes.

The shuttling rates observed herein for **UWDM-11**·(mesitylene) are still faster than our original observation of this process in the Zn-based MOF **UWDM-4**. This can be attributed to the larger cavities of **UWDM-11**, which is based on the **fcu** MOF **PCN-57** of the **UiO-68** family. Furthermore, **PCN-57** contains two types of cavities, tetrahedral and octahedral, of which only the latter contains the molecular shuttle. The ease of movement of the mesitylene guest molecules between the octahedral cavities containing the molecular shuttle and the vacant tetrahedral cavities may also minimise the blocking effect of the guest molecules on the shuttling of the macrocycle.

In the case of a degenerate molecular shuttle, like those previously reported by our group, when the rate of shuttling is slower than the NMR timescale, two peaks of equal intensity are observed. However, **3** and **UWDM-11** are non-degenerate with two chemically distinct recognition sites; the terphenyl stoppered site **a** and the dibromo stoppered site **b**. As indicated by the solution NMR experiments, binding of the macrocycle at site **a** is more energetically favourable. The SSNMR spectra for **UWDM-11**·(mesitylene) are further evidence for this because the proportion of the peak at 151.1 ppm corresponding to the binding of the crown ether macrocycle is significantly larger than the peak at 148.3 ppm, which indicates site **a** is more energetically favourable (78% at 173 K) than site **b** (22% at 170 K, Fig. S25 and S27†). These estimates of populations are approximate, based on the assumption that the peak intensities can be treated as quantitative measures of the populations of the two sites, since the ^{1}H–^{13}C CP process involves the same ^{13}C-enriched site in each case. It is possible there is some small variation in CP efficiency as the crown ether is positioned closer to and further from the ^{13}C-enriched site, though this would not be expected to be a major variation that would influence our analysis. As the ring has a greater preference for one of the sites, the rates of exchange from site **a** to site **b** and site **b** to site **a** are not identical. The site **b** to site **a** translation is faster as there is a lower activation barrier when the macrocycle leaves site **b**.[5d]

The translation of the macrocycle in a non-degenerate molecular shuttle (Fig. 5a) can be described by an asymmetric double well potential (Fig. 5b).[18] As the activation barrier for the site **a** to site **b** translation is larger, the rate is slower compared to the opposite translation. The rates for the site **a** to site **b** ($k_{\mathbf{a}}$) and site **b** to site **a** ($k_{\mathbf{b}}$) translations (Fig. 5a) and the corresponding free energies of activation, $\Delta G^{\ddagger}_{\mathbf{a}}$ and $\Delta G^{\ddagger}_{\mathbf{b}}$ (Fig. 5b), can be elucidated using the coalescence method. This method was modified to account for the uneven occupation of site **a** and site **b** (see ESI† for full details). The rates $k_{\mathbf{a}}$ and $k_{\mathbf{b}}$ at coalescence (273 K) are 162.3 and 575.3 s^{-1}, respectively while $\Delta G^{\ddagger}_{\mathbf{a}}$ and $\Delta G^{\ddagger}_{\mathbf{b}}$ are 13.2 and 12.5 kcal mol^{-1} respectively. These values are comparable to that obtained for **UWDM-4**, which also contains guest molecules in the pores.[10h] Although, the shuttling rates inside solvent-free **UWDM-11** could not be measured, an upper limit for $\Delta G^{\ddagger}_{\mathbf{a}}$ and $\Delta G^{\ddagger}_{\mathbf{b}}$ can be estimated (see ESI for details; Fig. S26 and Table S5†) based on the assumption that the highest possible temperature that coalescence could occur is the lowest temperature measured (*i.e.*, 173 K). This estimate results in values for the upper limit for $\Delta G^{\ddagger}_{\mathbf{a}}$ and $\Delta G^{\ddagger}_{\mathbf{b}}$ of 8.19 and 7.76 kcal mol^{-1} respectively, significantly lower than determined for **UWDM-11**·(mesitylene) (see ESI† for detailed comparison of shuttling rates in MOFs; Table S6†). This can be attributed to differences in the effective viscosities of the surrounding environments for the macrocycles in **UWDM-11** and **UWDM-11**·(mesitylene).

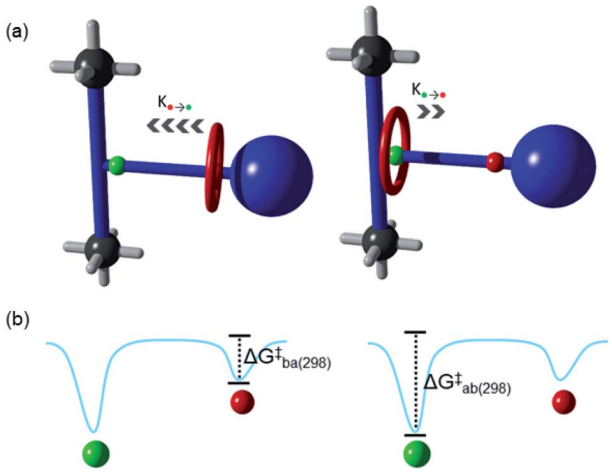

Fig. 5 (a) Schematic representation of the two translational processes occurring for the degenerate molecular shuttle inside the MOF; the shuttling of the ring from site **a** (●) to site **b** (●) and *vice versa*. (b) These translations can be described using an asymmetric, double-well double-potential with two activation energy barriers of different heights, $\Delta G^{\ddagger}_{\mathbf{a}}$ and $\Delta G^{\ddagger}_{\mathbf{b}}$.

Conclusions

A new design for imbedding [2]rotaxane linkers into multivariate Zr(IV) MOFs has been successfully implemented. This strategy allowed for a non-degenerate molecular shuttle to be incorporated into the octahedral cavity of a **UiO-68**/**PCN-57** analogue, **UWDM-11**. The molecular shuttle exhibits fast translation of the macrocycle when in solution or placed inside a MOF (**UWDM-11**) that has been fully activated (*i.e.*, solvent-free cavities). However, upon adsorption of mesitylene guest molecules into the pores of **UWDM-11**, the rate of translation slows sufficiently such that VT SSNMR spectroscopy can be used to elucidate the rates and energy barriers of translation. Importantly, this demonstrates the importance of guest molecules on the translational motion of [2]rotaxane molecular shuttles in MOFs and contrasts with the very limited observed effect of solvent on the rotation of the macrocycle in related solid-state systems.[10b]

Due to the unsymmetrical nature of the non-degenerate molecular shuttle, there are two different energy barriers, and one of the axle recognition sites displays a higher affinity for the macrocyclic wheel. Since binary molecular switches can be constructed from non-degenerate molecular shuttles by using an external stimulus to invert the thermodynamic preferences of the ring position, the results described herein can be used for

the development of MOFs containing molecular switches based on this new MIM linker design.

Author contributions

Conceptualization, S. J. L. and B. H. W.; investigation – MOFs, B. H. W.; investigation – SSNMR; L. M. A.; formal analysis – SSNMR, B. H. W., L. M. A. and R. W. S.; writing – original draft, B. H. W., S. J. L.; writing – review & editing, S. J. L., R. W. S., B. H. W. and L. M. A.; funding acquisition, S. J. L. and R. W. S.

Conflicts of interest

There are no conflicts to declare.

Acknowledgements

S. J. L. acknowledges the Natural Sciences and Engineering Research Council of Canada for support of a Discovery Grant (RGPIN-2018_101694) and a Canada Research Chair. R. W. S. is grateful for research support from The Florida State University and the National High Magnetic Field Laboratory (NHMFL), which is funded by the National Science Foundation Cooperative Agreement (DMR-1644779) and by the State of Florida. R. W. S. also thanks the University of Windsor, the Canadian Foundation for Innovation, and the Ontario Innovation Trust for support of the solid-state NMR facilities at Windsor, and Natural Sciences and Engineering Research Council for a Discovery Grant (RGPIN-2016_06642).

Notes and references

1 C. J. Bruns and J. F. Stoddart, *The Nature of the Mechanical Bond: From Molecules to Machines*, John Wiley & Sons, 2016.

2 (*a*) D. Sluysmans and J. F. Stoddart, *Trends Chem.*, 2019, **1**, 185–197; (*b*) M. Xue, Y. Yang, X. Chi, X. Yan and F. Huang, *Chem. Rev.*, 2015, **115**, 7398–7501.

3 (*a*) R. A. Bissell, E. Córdova, A. E. Kaifer and J. F. Stoddart, *Nature*, 1994, **369**, 133–137; (*b*) P. L. Anelli, N. Spencer and J. F. Stoddart, *J. Am. Chem. Soc.*, 1991, **113**, 5131–5133.

4 (*a*) D. D. Günbaş and A. M. Brouwer, *J. Org. Chem.*, 2012, **77**, 5724–5735; (*b*) P. G. Young, K. Hirose and Y. Tobe, *J. Am. Chem. Soc.*, 2014, **136**, 7899–7906.

5 (*a*) S. Silvi, M. Venturi and A. Credi, *J. Mater. Chem.*, 2009, **19**, 2279–2294; (*b*) J. Berná, M. Alajarín, C. Marín-Rodríguez and C. Franco-Pujante, *Chem. Sci.*, 2012, **3**, 2314–2320; (*c*) B. José, B. Giovanni, A. L. David and M. P. Emilio, *Pure Appl. Chem.*, 2007, **79**, 39–54; (*d*) N. Farahani, K. Zhu and S. J. Loeb, *ChemPhysChem*, 2016, **17**, 1875–1880; (*e*) H. Fu, X. Shao, C. Chipot and W. Cai, *Chem. Sci.*, 2017, **8**, 5087–5094.

6 (*a*) G. Gholami, K. Zhu, G. Baggi, E. Schott, X. Zarate and S. J. Loeb, *Chem. Sci.*, 2017, **8**, 7718–7723; (*b*) K. Zhu, V. N. Vukotic and S. J. Loeb, *Angew. Chem., Int. Ed.*, 2012, **51**, 2168–2172; (*c*) K. Zhu, V. N. Vukotic, N. Noujeim and S. J. Loeb, *Chem. Sci.*, 2012, **3**, 3265–3271.

7 (*a*) S. Mena-Hernando and E. M. Pérez, *Chem. Soc. Rev.*, 2019, **48**, 5016–5032; (*b*) B. H. Wilson and S. J. Loeb, *Chem*, 2020, **6**, 1604–1612.

8 (*a*) H. Deng, M. A. Olson, J. F. Stoddart and O. M. Yaghi, *Nat. Chem.*, 2010, **2**, 439–443; (*b*) S. J. Loeb, *Chem. Commun.*, 2005, 1511–1518; (*c*) S. J. Loeb, *Chem. Soc. Rev.*, 2007, **36**, 226–235; (*d*) P. Martinez-Bulit, A. J. Stirk and S. J. Loeb, *Trends Chem.*, 2019, **1**, 588–600.

9 (*a*) X. Jiang, H.-B. Duan, S. I. Khan and M. A. Garcia-Garibay, *ACS Cent. Sci.*, 2016, **2**, 608–613; (*b*) J. Perego, S. Bracco, M. Negroni, C. X. Bezuidenhout, G. Prando, P. Carretta, A. Comotti and P. Sozzani, *Nat. Chem.*, 2020, **12**, 845–851.

10 (*a*) N. Farahani, K. Zhu, C. A. O'Keefe, R. W. Schurko and S. J. Loeb, *ChemPlusChem*, 2016, **81**, 836–841; (*b*) P. Martinez-Bulit, C. A. O'Keefe, K. Zhu, R. W. Schurko and S. J. Loeb, *Cryst. Growth Des.*, 2019, **19**, 5679–5685; (*c*) D. J. Mercer, J. Yacoub, K. Zhu, S. K. Loeb and S. J. Loeb, *Org. Biomol. Chem.*, 2012, **10**, 6094–6104; (*d*) V. N. Vukotic, K. J. Harris, K. Zhu, R. W. Schurko and S. J. Loeb, *Nat. Chem.*, 2012, **4**, 456–460; (*e*) V. N. Vukotic and S. J. Loeb, *Chem. Soc. Rev.*, 2012, **41**, 5896–5906; (*f*) V. N. Vukotic, C. A. O'Keefe, K. Zhu, K. J. Harris, C. To, R. W. Schurko and S. J. Loeb, *J. Am. Chem. Soc.*, 2015, **137**, 9643–9651; (*g*) K. Zhu and S. J. Loeb, Organizing Mechanically Interlocked Molecules to Function Inside Metal–Organic Frameworks, in *Molecular Machines and Motors: Recent Advances and Perspectives*, ed. Credi, A., Silvi, S. and Venturi, M., Springer International Publishing, Cham, 2014; pp. 213–251; (*h*) K. Zhu, C. A. O'Keefe, V. N. Vukotic, R. W. Schurko and S. J. Loeb, *Nat. Chem.*, 2015, **7**, 514–519; (*i*) K. Zhu, V. N. Vukotic, C. A. O'Keefe, R. W. Schurko and S. J. Loeb, *J. Am. Chem. Soc.*, 2014, **136**, 7403–7409; (*j*) P. R. McGonigal, P. Deria, I. Hod, P. Z. Moghadam, A.-J. Avestro, N. E. Horwitz, I. C. Gibbs-Hall, A. K. Blackburn, D. Chen, Y. Y. Botros, M. R. Wasielewski, R. Q. Snurr, J. T. Hupp, O. K. Farha and J. F. Stoddart, *Proc. Natl. Acad. Sci. U. S. A.*, 2015, **112**, 11161.

11 (*a*) G. Gholami, B. H. Wilson, K. Zhu, C. A. O'Keefe, R. W. Schurko and S. J. Loeb, *Faraday Discuss.*, 2020, DOI: 10.1039/d0fd00004c; (*b*) B. H. Wilson, C. S. Vojvodin, G. Gholami, L. M. Abdulla, R. W. Schurko and S. J. Loeb, *Chem*, 2021, **7**, 202–211.

12 (*a*) A. J. Howarth, Y. Liu, P. Li, Z. Li, T. C. Wang, J. T. Hupp and O. K. Farha, *Nat. Rev. Mater.*, 2016, **1**, 15018; (*b*) S. Yuan, J.-S. Qin, C. T. Lollar and H.-C. Zhou, *ACS Cent. Sci.*, 2018, **4**, 440–450; (*c*) C. Healy, K. M. Patil, B. H. Wilson, L. Hermanspahn, N. C. Harvey-Reid, B. I. Howard, C. Kleinjan, J. Kolien, F. Payet, S. G. Telfer, P. E. Kruger and T. D. Bennett, *Coord. Chem. Rev.*, 2020, **419**, 213–388.

13 (*a*) P. R. Ashton, R. Ballardini, V. Balzani, I. Baxter, A. Credi, M. C. T. Fyfe, M. T. Gandolfi, M. Gómez-López, M. V. Martínez-Díaz, A. Piersanti, N. Spencer, J. F. Stoddart, M. Venturi, A. J. P. White and D. J. Williams, *J. Am. Chem. Soc.*, 1998, **120**, 11932–11942; (*b*) D. A. Leigh and A. R. Thomson, *Org. Lett.*, 2006, **8**, 5377–5379.

14 K. Zhu, V. N. Vukotic and S. J. Loeb, *Chem.–Asian J.*, 2016, **11**, 3258–3266.
15 (*a*) J. H. Cavka, S. Jakobsen, U. Olsbye, N. Guillou, C. Lamberti, S. Bordiga and K. P. Lillerud, *J. Am. Chem. Soc.*, 2008, **130**, 13850–13851; (*b*) H.-L. Jiang, D. Feng, T.-F. Liu, J.-R. Li and H.-C. Zhou, *J. Am. Chem. Soc.*, 2012, **134**, 14690–14693.
16 N. Noujeim, K. Zhu, V. N. Vukotic and S. J. Loeb, *Org. Lett.*, 2012, **14**, 2484–2487.
17 *BIOVIA Materials Studio*, 2019.
18 D. A. Leigh, A. Troisi and F. Zerbetto, *Angew. Chem., Int. Ed.*, 2000, **39**, 350–353.